

Nucleation dynamics around single microabsorbers in water heated by nanosecond laser irradiation

Jörg Neumann^{a)} and Ralf Brinkmann

Medizinisches Laserzentrum Lübeck GmbH, Peter-Monnik-Weg 4, D-23562 Lübeck, Germany

(Received 30 August 2006; accepted 28 March 2007; published online 8 June 2007)

Suspensions containing micro- and nanoabsorbers, which are irradiated by short laser pulses, are used for a manifold of procedures in medicine, biotechnology, and other fields. Detailed knowledge of the bubble nucleation and dynamics, which is induced by the heat transfer from the absorber to the surrounding transparent water, is essential for understanding the underlying processes occurring on a microscopic scale. We investigated the rapid phase change phenomena including temperature, heating rates, pressure generation, bubble nucleation, and initial bubble growth around absorbing micron-sized melanin particles (retinal pigment epithelial melanosomes) during irradiation with 12 ns (full width at half maximum) laser pulses at a wavelength of 532 nm. The melanosomes were heated at rates in the order of 10^{10} K/s. A mean bubble nucleation temperature of 136 °C was found. The initial bubble expansion was observed by time-resolved microscopy. The expansion velocities range from 10 m/s at 1.5-fold to 85 m/s at 8.5-fold threshold radiant exposure for bubble formation, respectively. The expansion velocity increases in the investigated range almost linearly with the applied radiant exposure. © 2007 American Institute of Physics.

[DOI: [10.1063/1.2740348](https://doi.org/10.1063/1.2740348)]

I. INTRODUCTION

The early stages of rapid phase change of fluids in contact with a solid surface, which is heated at rates as high as 10^{10} K/s, are mainly unexplored. Rapid vaporization of a fluid at a heated solid surface occurs in many laser-assisted medical treatment modalities such as selective retina treatment¹⁻³ (SRT) and selective laser trabeculoplasty⁴ (SLT) as well as in biomedical procedures such as nanoparticle assisted cellular surgery and selective cell killing.⁵⁻⁷ Technical applications comprise bubble jet printer technologies,⁸ steam laser cleaning,⁹ bubble induced optical limiting in suspensions,¹⁰ transient holographic gratings,^{11,12} as well as bubble mediated fast optical switching¹³ and surface assisted laser desorption ionization (SALDI).^{14,15} Furthermore, a phase transition of a fluid in the vicinity of a rapidly heated surface plays a major role in laser-induced triggering of chemical reactions in suspensions containing micro- and nanoabsorbers,¹⁶ because it can provide gaseous micro- and nanoenvironments with unique properties such as high temperatures and pressures localized inside the bubble around the absorber without producing any significant increase of the mean suspension temperature and pressure.¹⁶⁻¹⁸

Time-resolved microscopy has been applied for optimization of ink jet printer technologies.¹⁹⁻²¹ With respect to optical limiting, laser-induced bubble formation in suspensions has been investigated experimentally by light scattering techniques^{22,23} and (macroscopic) shadowgraphic photography,^{24,25} which, however, was not applied with a submicron optical resolution. Only a few experimental, non-systematic studies on bubble formation around single spherical absorbers using time-resolved microscopy as well as light

scattering²⁶⁻²⁹ and x-ray scattering techniques^{30,31} are available up to date. The mechanisms, which lead to bubble formation at the absorbers, are vaporization of the solvent around the absorber and sublimation of the absorber itself.³²

As a contribution to an improved quantitative understanding of these processes, which involve bubble formation around single absorbing particles, models for the solvent vaporization around the absorber were developed,³³⁻³⁵ which have not been verified by experiments on the microscopic scale.

The aim of this study is to investigate the nucleation process and the initial bubble expansion around a single micron-sized absorber following nanosecond laser irradiation. These results can give essential information on the phase change phenomena in the fluid at rapidly heated solid interfaces as well as on the subsequent bubble dynamics. As strong absorbers, melanin containing melanosomes from the retinal pigment epithelium (RPE) were chosen with respect to pulsed laser applications at the retina such as SRT (Ref. 36) and other melanin containing ocular tissues such as the pigmented trabecular meshwork, which is targeted in SLT.⁴ For SLT (glaucoma treatment), the trabecular meshwork at the anterior chamber of the eye is irradiated by laser pulses with a duration of a few nanoseconds at a wavelength of 532 nm in order to selectively damage the pigmented tissue by transient microbubble formation around the absorbing micron-sized intracellular melanosomes. For SRT, which is applied to treat several retinal disorders,³⁶ transient bubble formation around melanosomes is used to selectively damage retinal pigment epithelial cells while sparing the adjacent photoreceptor cells. Currently 1.7 μ s pulses are used, but the optimum pulse duration is still unknown.³⁷ Nanosecond laser pulses are easier to generate from the technical point of view and might also be appropriate for SRT. Therefore, it is required to investigate the thermomechanical effects induced

^{a)}Author to whom correspondence should be addressed; FAX: +49-511-2788-100; electronic mail: j.neumann@lzh.de

by nanosecond irradiation of the strongly absorbing melanosomes, because cells, which contain these absorbers, are targeted in SRT and SLT. Moreover, nanosecond pulse duration was chosen, because it goes along with thermally confined but inertially unconfined irradiation of the melanosomes, i.e., selective heating of melanosomes under prevention of potentially damaging strong acoustic transients.³⁸ The damage range in the tissue, which is in this case mainly determined by the transient laser-induced bubbles around the absorbers, is crucial in SRT to prevent irreversible damage to the retinal photoreceptors (Refs. 1–3, 39, and 40) and has also strong implications for laser eye safety issues.³⁴

II. MATERIAL AND METHODS

The melanosomes are harvested from the retinal pigment epithelium of enucleated porcine eyes,³⁸ which are obtained from a local abattoir. After equatorial dissection of the eyes, the anterior part and the vitreous are removed. Purified, degassed, and demineralized water is added. After a few minutes, the neural retina can be detached. Subsequently, the superficial RPE cell layer is removed by a stiff brush and purified by filter paper (Schleicher & Schüll 595 1/2, retention range of 4–7 μm) to separate the melanosomes from cellular debris. As observed by light microscopy, porcine melanosomes are rotational ellipsoidal with mean diameters of $d_1=d_2=0.8\pm 0.1\ \mu\text{m}$ and $d_3=2.3\pm 0.6\ \mu\text{m}$. The main constituent and chromophore of melanosomes is the polymer melanin. The absorption of melanin is monotonically decreasing with wavelength in the visible spectral range.⁴¹ For the experiments, 25 μl of the aqueous melanosome suspension are given on an object slide. The fluid reservoir is prevented from drying by using gene frames (ABgene, United Kingdom), which seal the reservoir and keep a distance of about 250 μm between the object slide and cover slip. Temperature-dependent measurements are performed in a cuvette with a depth of 4 mm, which enables us to adequately place the thermocouple of a digital thermometer (Lutron TM-914C, type-K thermocouple) for measurement of the bulk suspension temperature. For immobilization of the particles in the cuvette, 0.1% of agarose is added to the suspension. The cuvette can be heated electrically by a resistor and cooled by a thermoelectric cooler.

The experimental setup for irradiation of the melanosomes and observation of the bubble formation is depicted in Fig. 1. The aqueous melanosome suspension is observed by means of a video microscope. We use a standard 40 \times microscope objective with a numerical aperture of $\text{NA}=0.65$, which provides an optical resolving power of about 0.5 μm . The melanosomes are irradiated by a frequency doubled Q -switched Nd:YAG (neodymium yttrium aluminum garnet) laser (Spectron Lasersystems SL401). An aperture has been inserted into the laser cavity to prevent oscillations of higher order modes. Operating the laser slightly above lasing threshold, a full width at half maximum (FWHM) pulse duration of 12 ns has been achieved at a wavelength of 532 nm. The laser is always operated at the same set of parameters to perform all experiments with the same temporal pulse shape. The laser pulses are transmitted by a multimode fiber (Ceram

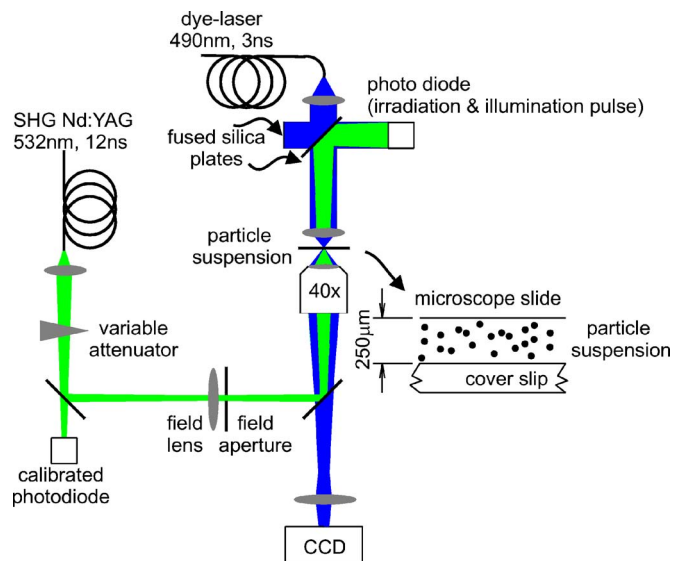


FIG. 1. (Color online) Experimental setup for nanosecond time-resolved microscopy of bubble formation around individual laser-heated melanosomes.

Optec, Optron UV-A 105/125A/250) with a core diameter of 105 μm and a numerical aperture of $\text{NA}=0.22$. The laser pulses are attenuated before fiber transmission to prevent wavelength shifts in the fiber due to Raman scattering. The transmitted pulse energy is less than 20 μJ . It is measured by an energy meter (Ophir Optronics, Laserstar PE 10) behind the first lens at the fiber output. A fiber length of 200 m has been chosen to reduce spatial intensity modulation due to speckles below 15%. The pulse energy is adjusted by a variable attenuator (Fig. 1). A photodiode (Centronics, AEPX 65) with a current integrating circuit is used to determine the laser pulse energy, calibrated to an energy meter (Ophir Optronics, Laserstar PE 10). A top hat beam profile at the specimen with a diameter of 39.5 μm is achieved by mapping the fiber tip into the suspension. For determination of the spot size, the melanosome suspension has been replaced by a reflecting slide micrometer scale. The laser spot on the scale is observed with a charge coupled device (CCD) camera (Fig. 1). Fast flash photographs with an optical resolution of about 0.5 μm are taken by the CCD camera (JAI A/S, Denmark, CV-A11) and a frame grabber (National Instruments, IMAQ 1409) interfaced to a personal computer. A N_2 -laser pumped dye laser (Laser Science, VSL-337-ND, DLM220) with a pulse duration of 3 ns serves as flash. The pulse duration was determined in a separate setup with a fast photodiode (EG&G, FND-100Q, rise time $<1\ \text{ns}$, bandwidth: 350 MHz). Using the dye coumarin 102, the laser emission wavelength is tuned by an internal grating to 490 nm. Scattered light of the Nd:YAG laser is blocked by a short pass filter in front of the CCD camera. No major blurring of the bubble images is expected for bubble expansion velocities of less than 0.5 $\mu\text{m}/3\ \text{ns}=150\ \text{m/s}$ due to the short illumination pulse duration. The pulse energy of the dye laser at the particle suspension is below 1 μJ on the 200 μm diameter illumination spot, which results in a radiant exposure of less than 3 mJ/cm^2 . The dye laser is triggered with an adjustable delay related to the irradiation pulse of the Nd:YAG laser.

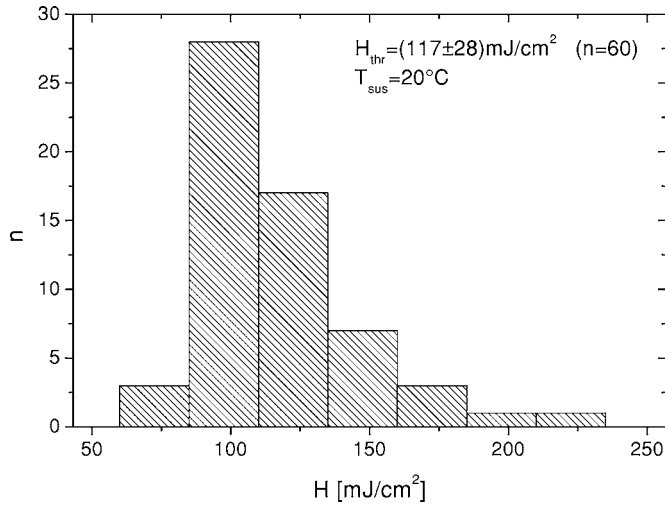


FIG. 2. (Color online) Distribution of threshold radiant exposures for bubble formation obtained at a suspension temperature of 20 °C from $n=60$ individual melanosomes.

Irradiation and illumination pulses are monitored by the same photodiode (Centronics, AEPX 65). The irradiation and the illumination pulse shapes as well as the calibrated photodiode voltage are recorded by a digital oscilloscope (LeCroy, Waverunner LT374).

III. RESULTS AND DISCUSSION

A. Bubble nucleation

To determine the threshold radiant exposure for bubble formation, the illumination pulse for photography is set to a delay of a few tens of nanoseconds related to the Nd:YAG laser pulse, which ensures photographic detection of all occurring laser-induced microbubbles. Light scattering techniques revealed in previous studies that the minimum bubble lifetime around a melanosome is about 50 ns for 12 ns laser

pulses.^{27,38} For these light scattering measurements, the bubbles with minimum detected lifetime show a good signal-to-noise ratio (Fig. 2 in Ref. 27 and Fig. 2 in Ref. 38), which is well above the detection capabilities of the experimental setup. These bubbles are simultaneously observable by photography. Therefore, it is assumed that for micron-sized particles there is a well-defined bubble threshold accompanied by a minimum bubble size, which is well above the detection sensitivity of the setup. Varying the radiant exposure at the variable attenuator, the bubble formation threshold for an individual melanosome does not show any pulse-to-pulse variations and can therefore be determined with an error of less than 5 mJ/cm², whereas the thresholds between distinct melanosomes vary within a range of a few tens of mJ/cm² (Fig. 2). The large variation in the bubble formation threshold between individual melanosomes can be explained by the varying melanosome properties such as size, ellipticity, position toward the laser source, etc., which have an impact on the melanosome heating. Moreover, the bubble nucleation temperature might differ from melanosome to melanosome, which also leads to a variation in bubble formation thresholds. At a suspension temperature of 20 °C a mean threshold radiant exposure for bubble formation of $H_{thr}=117$ mJ/cm² with a standard deviation of ± 28 mJ/cm² is averaged from $n=60$ individual melanosomes (Fig. 2).

The bubble nucleation temperature is obtained from temperature-dependent threshold measurements for bubble formation. For inertially unconfined laser irradiation, the influence of the thermoelastic pressure generation on nucleation is usually negligible at threshold radiant exposure for bubble formation (see Sec. III B) and heat generation determines the bubble nucleation. For nucleation, it is required that the initial surface temperature of the melanosome T_{sus} , which is at bulk suspension temperature, is increased by the laser pulse (ΔT_{laser}) to the nucleation temperature $T_{nuc}=T_{sus} + \Delta T_{laser}$. The corresponding phase diagram is depicted in

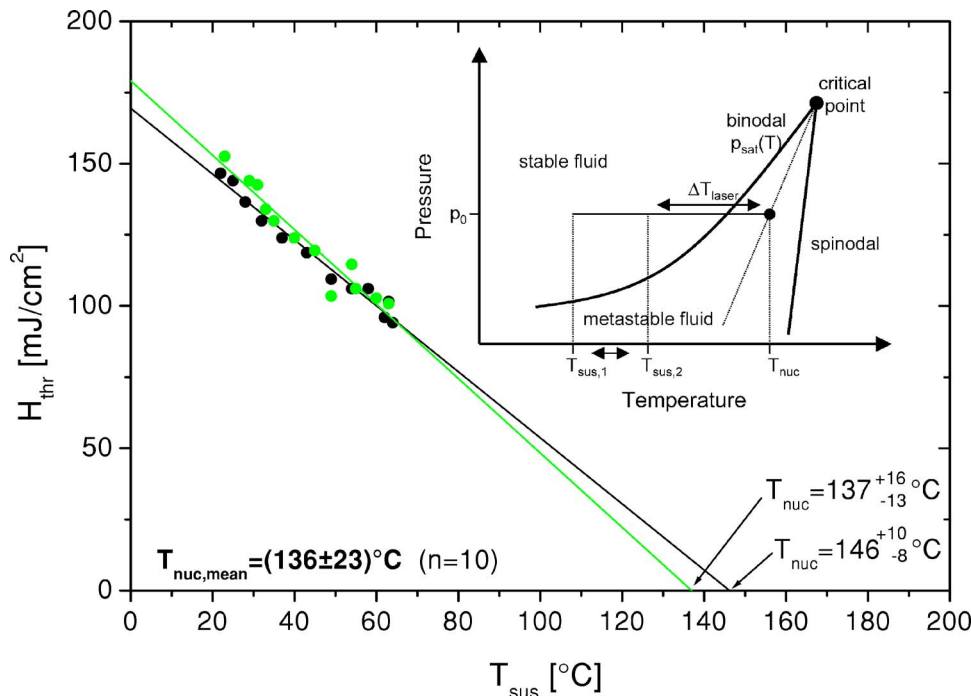


FIG. 3. (Color online) Representative temperature-dependent bubble threshold measurements for two individual melanosomes. The threshold radiant exposure for bubble formation decreases when the temperature of the suspension is increased, because less laser-induced heating is required to reach the nucleation temperature T_{nuc} . The value of T_{nuc} can be deduced for each melanosome from the intersection of the extrapolated linear fit and the temperature axis. A mean value of $T_{nuc}=(136\pm 23)$ °C is obtained by averaging the nucleation temperatures of $n=10$ individual melanosomes. The small graph shows the corresponding phase diagram. The bubble nucleation temperature is located between the binodal and the spinodal of water.

TABLE I. Properties of a melanosome with corresponding references.

	ρ (kg/m ³)	c_p (J/kg K)	κ (m ² /s)	c_l (m/s)	Γ
Melanosome	1410 (Ref. 58)	2550 (Ref. 60)	1.4×10^{-7} (Ref. 61)	$\sim 1500^a$ (Ref. 51)	$\sim 1^a$ (Ref. 52)

^aSince the velocity of sound in melanin and the Grüneisen parameter are not known, typical values for polymers are used (Refs. 51 and 52).

Fig. 3. If the temperature of the melanosome suspension is increased, less absorbed energy is needed to cause bubble formation, i.e., to reach the nucleation temperature T_{nuc} on the melanosome surface. Reviewing the equation of state (EOS) of water according to the International Association for Properties of Water and Steam (IAPWS-95) formulation⁴² in the stable and using data given by Skripov *et al.* in the metastable domain,⁴³ the isobaric volumetric heat capacity ρc_p for water at ambient pressure $p_0=1$ bar changes in the temperature range of 20–300 °C less than 10% relative to the value of ρc_p at 20 °C. Furthermore, the thermal conductivity of water K according to the IAPWS (Ref. 44) and its extrapolation in the metastable range was used to calculate the thermal diffusivity $\kappa=K/(\rho c_p)$. The relative variation of the thermal diffusivity of water is less than 20% in the temperature interval of 20–300 °C. However, for thermally confined irradiation, the influence of the thermal diffusivity κ is negligible and the governing property is the isobaric volumetric heat capacity ρc_p . Therefore, we neglect the temperature dependency of the thermal properties κ and ρc_p for the calculations. The properties of the melanosome are listed in Table I. Due to the resulting linearity of the heat conduction equation ($\Delta T_{\text{laser}} \propto H_{\text{thr}}$), the linear relationship $H_{\text{thr}}(T_{\text{sus}}) \propto \Delta T_{\text{laser}} = T_{\text{nuc}} - T_{\text{sus}}$ can be extrapolated to the nucleation temperature, where no additional laser energy is required to initiate vaporization, i.e., $T_{\text{sus}} = T_{\text{nuc}}$ at $H_{\text{thr}}(T_{\text{nuc}}) = 0$.^{38,45} In order to obtain the nucleation temperature of a melanosome, the same melanosome is irradiated at various suspension temperatures. The nucleation temperature can be obtained at the intersec-

tion of the extrapolated linear fit and the temperature axis [Fig. 3: $H_{\text{thr}}(T_{\text{nuc}}) = 0$]. The typical standard error for the determination of the nucleation temperature of a single melanosome is in most cases in the range between 10 and 15 °C. Averaging the results of $n=10$ individual melanosomes, a mean nucleation temperature of $T_{\text{nuc}} = 136$ °C with a standard deviation of ± 23 °C was found for 12 ns pulses at bubble formation threshold radiant exposure (Fig. 3).

The temporal evolution of the expanding bubbles is photographed at various time delays for three different super-threshold radiant exposures of 180 mJ/cm², 460 mJ/cm², and 1 J/cm². The resulting bubbles with typical lifetimes in the order of a microsecond have diameters of a few microns at the point of their maximum extension.²⁷ Observed by light microscopy, the melanosomes often show shape alterations after irradiation with radiant exposures exceeding 400 mJ/cm². Moreover, residual bubbles with lifetimes up to a few seconds can sometimes be observed after irradiation with more than 400 mJ/cm², which indicates that vaporization of the melanosome's constituents occurs. Consequently, for radiant exposures of 460 mJ/cm² and 1 J/cm² each melanosome was irradiated only once. For lower radiant exposures the superheated water layer around the particle vaporizes rather than the melanosome itself.³⁸ Figures 4–6 show exemplary photographs taken at different radiant exposures (180 mJ/cm², 460 mJ/cm², and 1 J/cm²) and at various time delays related to the Nd:YAG laser pulse. Application of half the laser pulse energy defines the zero point in time in Figs. 4–8. The bubble refracts the illumination light for pho-

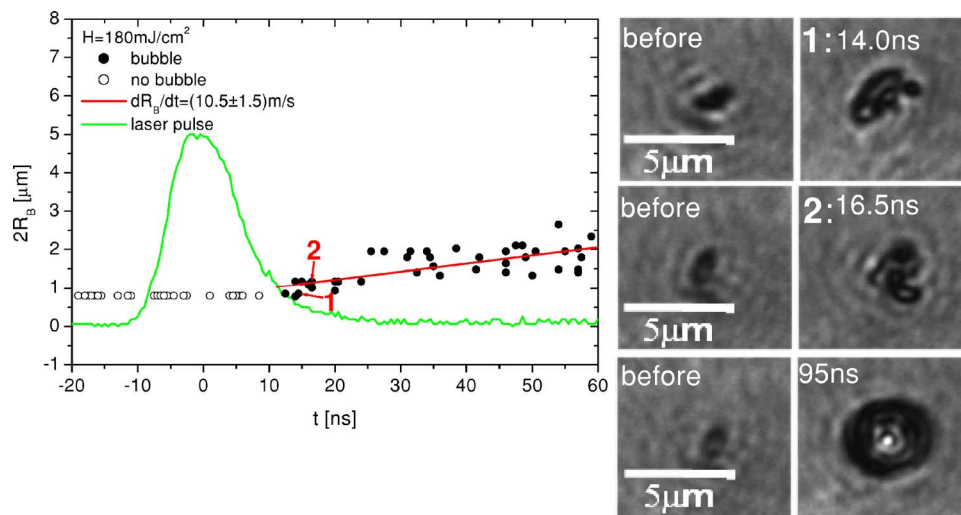


FIG. 4. (Color online) The temporal evolution of the bubble diameter $2R_b$, which is determined at a radiant exposure of 180 mJ/cm² by time-resolved microscopy, is displayed related to the laser pulse. The laser pulse amplitude is plotted in arbitrary units. At the origin of the time axis half the pulse energy was applied. The bubble expansion is approximated by a linear fit delivering a mean expansion velocity in the investigated time interval. Nucleation takes place between 8.5 and 12.5 ns on the time axis. Right: Representative photographs before (showing the melanosome) and after irradiation (showing bubbles) are depicted. (The point in time of photography, which is related to the time axis of the plot on the left, is displayed in the photographs as well. The numbers in the photographs correspond to the marked points in the graph.)

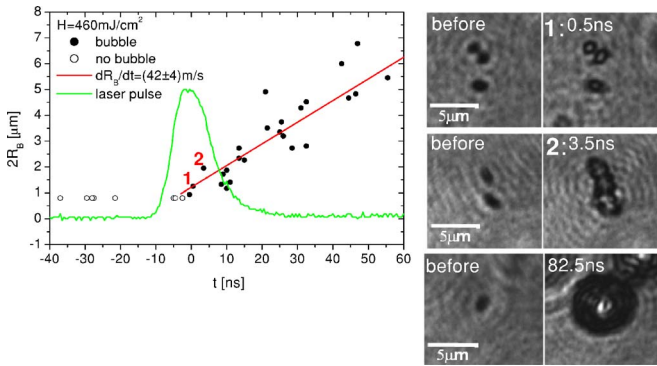


FIG. 5. (Color online) Bubble expansion around a melanosome at a radiant exposure of 460 mJ/cm^2 (see Fig. 4). Nucleation occurs between -2.5 and 0.5 ns.

topography out of the CCD camera's collection optics. Therefore, the bubbles appear dark on the photographs (Figs. 4–6). Since the size of the bubble is near the resolving power of the microscope, diffraction effects, which blur the image, occur. The plots in Figs. 4–6 display the diameters of the bubbles, which have been extracted from the photographs, versus the point of time, when the photograph was taken. For elliptical bubbles, the diameter in the axis with the smallest bubble extension is plotted in Figs. 4–6. If no bubble was observed on the photograph, the bubble diameter $2R_B$ was set to the mean diameter of the melanosome $d_1 = d_2 = 0.8 \text{ } \mu\text{m}$ and plotted as an open circle, whereas bubble formation is indicated as full circle.

To quantify the bubble expansion, a constant expansion velocity is assumed for simplicity during the first 60 ns after half the pulse energy deposition. The velocity is determined by a linear fit of the bubble diameters as a function of time. The bubble incipience is deduced from a series of images photographed at various delays. The point of nucleation can be restricted to the time interval between the last photograph without a bubble and the first revealing a bubble. With increasing radiant exposure, the bubble nucleates earlier relative to the laser pulse (Table II). At 180 mJ/cm^2 , which is 1.5-fold threshold irradiation for bubble formation, several nucleation sites can be observed in Fig. 4 (14 ns) and (16.5 ns) on the melanosome's surface. These individual bubbles growing on the melanosome's surface have coalesced in Fig. 4 (95 ns) to a single bubble surrounding the whole melanosome. The concept of overlapping bubbles,

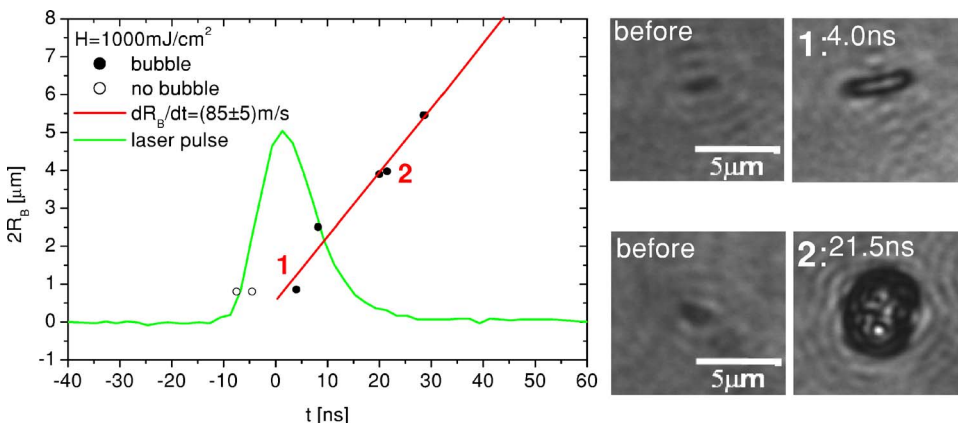


FIG. 6. (Color online) Bubble expansion around a melanosome at a radiant exposure of 1000 mJ/cm^2 (see Fig. 4). Nucleation occurs between -4.5 and 4.0 ns.

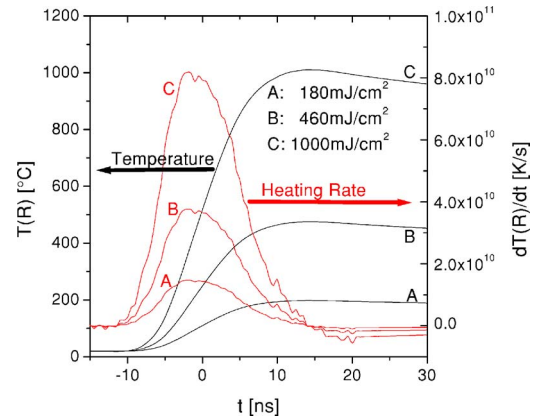


FIG. 7. (Color online) Calculated temperature and corresponding heating rate on the melanosome surface. Bubble formation, which leads to thermal insulation of the particle by the vapor inside the bubble, is not considered in the thermal model. Therefore, the model is only valid to the point where the bubble nucleation occurs.

which can lead to larger bubble diameters, has been analyzed by Zharov *et al.*⁴⁶ The existence of many nucleation sites at a radiant exposure of 180 mJ/cm^2 let us assume that inhomogeneous nucleation by surface imperfections, preexisting bubble nuclei or temperature induced production of small amounts of noncondensable gas such as CO_2 ,⁴⁷ takes place in this case. Inhomogeneous nucleation at a solid interface usually occurs below the spinodal limit of water T_{sp} (1 bar) $\approx 315 \text{ }^\circ\text{C}$,^{38,48,49} which is in agreement with a nucleation temperature of $T_{nuc} = (136 \pm 23) \text{ }^\circ\text{C}$ found for melanosomes at threshold radiant exposure. Nevertheless, compared to nucleation temperatures of water on clean and smooth metallic surfaces, which are in most cases between 200 and $300 \text{ }^\circ\text{C}$,^{19–21,38,43,49,50} the determined nucleation temperature for melanosomes is rather low and might be caused by preexisting bubble nuclei or temperature induced production of noncondensable gas.

In contrast to the observation of single nucleation sites (Fig. 4, 14 and 16.5 ns), a single bubble with a smooth surface around the whole melanosome can be seen in the early stages of the bubble growth at higher radiant exposures of 460 mJ/cm^2 and 1 J/cm^2 (Fig. 5, 0.5 and 3.5 ns and Fig. 6, 4.0 ns). Although a qualitative difference in the bubble nucleation between near threshold (180 mJ/cm^2) and high radiant exposure (460 mJ/cm^2 , 1 J/cm^2) is observed, both

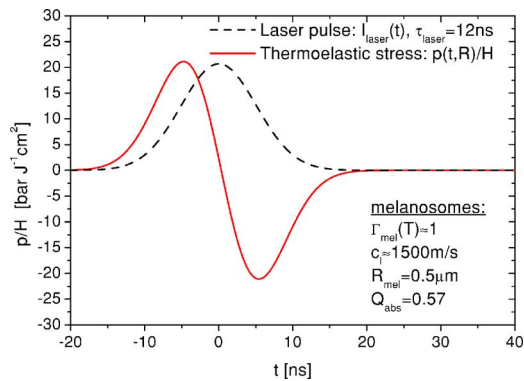


FIG. 8. (Color online) Thermoelastic stress generation at a single melanosome: Plot of the calculated transient pressure on the surface of the melanosome produced by a 12 ns pulse at a radiant exposure of 1 J/cm². The corresponding temporal laser pulse shape is also depicted.

nucleation modalities lead to a single bubble around the whole melanosome (Fig. 4, 95 ns; Fig. 5, 83.5 ns; and Fig. 6, 21.5 ns), if a sufficient amount of energy for bubble growth has been applied. Due to surface tension, the bubble surface area is minimized and the bubble becomes more spherical with size, i.e., in the later stages of bubble growth (Fig. 4, 95 ns; Fig. 5, 83.5 ns; and Fig. 6, 21.5 ns).

The time-dependent temperature on the surface of the melanosome and the heating rate at the time of nucleation are estimated in Fig. 7. For this reason, the semianalytic heat conduction model from Ref. 38 is employed, which solves the heat equation

$$\frac{\partial T}{\partial t} - \kappa \nabla^2 T = \frac{A}{\rho c_p} \quad (1)$$

(T , temperature; κ , thermal diffusivity; ρ , density; c_p , specific heat; and A , input power density, Table I) for different material properties between the melanosome and its surrounding (with boundary conditions of continuous temperature T and $\kappa \rho c_p (\partial T / \partial r)$ at the melanosome interface) and for arbitrary temporal pulse shapes. A spherical absorber with a radius of $R=0.5 \mu\text{m}$ and spatial homogeneous heat deposition is assumed. The initial temperature is set to 20 °C. The absorption efficiency of the melanosome, which is the ratio of absorbed laser pulse energy E_{abs} to the radiant exposure H passing the geometric cross section of the absorber πR^2 , is adjusted in the model to $Q_{\text{abs}}=E_{\text{abs}}/(H\pi R^2)=0.57$ in order to obtain the experimentally determined nucleation temperature of $T_{\text{nuc}}=136 \text{ °C}$ on the melanosome surface at a threshold radiant exposure of $H_{\text{thr}}=117 \text{ mJ/cm}^2$.

The plots of the surface temperature in Fig. 7 are differentiated with respect to time in order to approximate the heating rate on the melanosome's surface for the applied radiant exposures. Because the main purpose of this model is to describe the temperature and heating rate until the bubble nucleates, the thermal insulation of the particle from the surrounding water due to the vapor bubble is not incorporated.³³ Therefore, the model is only valid to the point when bubble nucleation occurs. The calculated temperature interval and the heating rate at the point of nucleation are listed in Table II. For the nucleation temperature at a threshold radiant exposure of $T_{\text{nuc}}=(136\pm 23) \text{ °C}$, the relative standard deviation of the temperature increase for nucleation is $23 \text{ °C}/(136-20 \text{ °C})=20\%$. The relative error of the determined absorption efficiency ($Q_{\text{abs}}=0.57$) due to the relative standard deviation of the threshold radiant exposure for bubble nucleation is $28 \text{ mJ/cm}^2/117 \text{ mJ/cm}^2=25\%$. Assuming that both relative errors are uncorrelated and remain constant with radiant exposure, they result in an overall relative error of $\sqrt{(25\%)^2+(20\%)^2}=32\%$ in temperature increase and heating rate (Fig. 7), which is accounted for in Table II, i.e., the minimum and maximum temperature increases and the corresponding heating rates on the melanosome's surface are calculated in the nucleation interval $[t_{\text{nuc,min}}, t_{\text{nuc,max}}]$ with the heat conduction model; subsequently, an additional relative error of $\pm 32\%$ is added.

B. Pressure generation

In contrast to irradiation of melanosomes with 30 ps pulses,²⁶ no change of the refractive index due to shock wave formation is observed on the microphotographs around the melanosome after 12 ns irradiation, even at a radiant exposure of 1 J/cm². The absence of shock waves indicates that only moderate pressure amplitudes are generated by the 12 ns pulsed laser irradiation.

However, there are two major sources of pressure, namely, the thermoelastic pressure, which is generated by the temperature induced volume expansion (without phase change), and the phase change induced pressure generation. The latter can be roughly estimated by the saturated vapor pressure at the nucleation temperature of $p_{\text{sat}}(136 \text{ °C})=3.2 \text{ bars}$. The thermoelastic pressure generation is calculated as follows: If the laser pulse duration τ_{laser} is shorter than the transit time τ_p of the pressure wave traveling through the particle, the condition of stress confinement is fulfilled. For a spherical melanosome with a radius of $R=0.5 \mu\text{m}$, stress confined irradiation requires a laser pulse

TABLE II. Time interval t_{nuc} , where nucleation occurs according to Figs. 4–6 as well as corresponding calculated nucleation temperatures $T_{\text{nuc}}(R, t_{\text{nuc}})$ and heating rates $dT/dt(R, t_{\text{nuc}})$ on the melanosome surface at the point of nucleation. The data have been extracted from Fig. 7.

H (mJ/cm ²)	t_{nuc} (ns)		$T_{\text{nuc}}(R, t_{\text{nuc}})$ (°C)		$dT/dt(R, t_{\text{nuc}})$ (10 ⁹ K/s)	
	min	max	min	max	min	max
180	8.5	12.5	136	254	0.7	4.6
460	−2.5	−0.5	89	305	25	49
1000	−4.5	4.0	101	1131	41	84

duration of $\tau_{\text{laser}} \ll 2R/c_{1l} = \tau_p \approx 2 \times 0.5 \mu\text{m}/1500 \text{ ns}^{-1} \approx 700 \text{ ps}$.³⁸ Because the speed of sound for longitudinal waves inside the melanosome c_{1l} is not available, we assume a value of $c_{1l} = 1500 \text{ m/s}$ (Table I), which is a typical value for polymers.⁵¹ Stress confined irradiation usually results in high pressure amplitudes.^{34,52} Although the condition of stress confinement is not fulfilled for 12 ns pulses, appreciable thermoelastic pressure amplitudes might be generated due to the laser irradiation. Because tensile stress can lead to a decrease of the nucleation temperature and can contribute to bubble nucleation (cold bubbles),^{52,53} we model the laser-induced generation of thermoelastic stress. The stress ampli-

tudes are only calculated in the surrounding water, because we observe no stress induced breakage of the melanosomes. The emitted pressure wave is calculated for a temporal Gaussian pulse shape (Fig. 8, compare experimental pulse shapes in Figs. 4–6) with an intensity of

$$I(t) = \frac{H}{\Theta_{\text{laser}} \sqrt{\pi}} \exp\left(-\frac{t^2}{\Theta_{\text{laser}}^2}\right), \quad (2)$$

where $\Theta_{\text{laser}} = 2\tau_{\text{laser}}/\sqrt{4 \ln 2} \approx 0.6\tau_{\text{laser}}$. τ_{laser} is the FWHM duration of the laser pulse. H is the spatially constant radiant exposure. According to Kahn and Diebold⁵⁴ the pressure outside the absorber ($r \geq R$) is given by

$$p(r,t) = H \frac{3Q_{\text{abs}} \beta c_{1l}^2 (2/3\sqrt{\pi})(\rho_2/\rho_1)(\tau_p/2\Theta_{\text{laser}})^3 [(c_{1l}/c_{2l}) - c_{1l}(t/r)]}{4R c_{1p} 1 - (2c_{1l}/c_{1l})^{2/3}} \exp\left\{-\frac{[t - (r/c_{2l})]^2}{\Theta_{\text{laser}}^2}\right\}, \quad \tau_p = \frac{2R}{c_{1l}}. \quad (3)$$

Properties of the medium inside the sphere are represented in Eq. (3) by the suffix 1; parameters of the aqueous surrounding are denoted by the suffix 2. ρ is the density. β is the volumetric thermal expansion coefficient. c_p is the isobaric heat capacity. c_l and c_t are the speeds of compressional (longitudinal) and shear (transversal) waves. We model the melanosome as a sphere with a radius of $R = 0.5 \mu\text{m}$ and use the same value for the absorption efficiency ($Q_{\text{abs}} = 0.57$) as in the thermal model. A Grüneisen parameter of $\Gamma = \beta c_{1l}^2 / c_{1p} = 1$ is chosen, which is a typical value for polymers.⁵² The exact value of the Grüneisen parameter for a melanosome is not known. Neglecting shear waves in the melanosome ($c_{1t} = 0$), we use for the speed of longitudinal waves $c_{1l} = 1500 \text{ m/s}$. The temperature dependencies of these constants are not considered.

The model of Kahn and Diebold is only valid if the melanosome is not irradiated under stress confinement conditions ($\tau_{\text{laser}} \gg \tau_p \approx 700 \text{ ps}$). Because the particles are irradiated in the regime of thermal confinement [$\tau_{\text{laser}} \ll \tau_T = R^2/4\kappa \approx 450 \text{ ns}$ (Ref. 38)], heat diffusion is negligible and therefore not incorporated in the pressure model. In addition, homogeneous heating of the spherical particle is assumed, which is a reasonable approximation.³⁸

For the melanosome, which is irradiated by a 12 ns pulse, we calculate pressure amplitudes per radiant exposure of $p/H = \pm 21 \text{ bars}/(\text{J}/\text{cm}^2)$ on the melanosome's surface (Fig. 8). According to Eq. (3) the maximum amplitudes for compressive and tensile stress have the same absolute value. At threshold radiant exposure for bubble formation $H_{\text{thr}} = 117 \text{ mJ}/\text{cm}^2$, a pressure amplitude of $p = \pm 2.5 \text{ bars}$ is calculated; 180, 460, and $1000 \text{ mJ}/\text{cm}^2$ result in 3.8, 9.7, and 21.1 bars, respectively, at the melanosome surface. These values are comparable to the saturated vapor pressure of $p_{\text{sat}}(136 \text{ }^\circ\text{C}) = 3.2 \text{ bars}$ at the experimentally determined nucleation temperature and can therefore increase the required nucleation temperature during the phase of compressive stress and decrease the nucleation temperature during

tensile stress. As a consequence, the bubble nucleation process might be influenced by the thermoelastic pressure generation. In Figs. 4–6 bubble formation is only observed after the maximum of the laser pulse, where tensile stress occurs (Fig. 8). On the other hand, previous experiments have revealed that the point in time, when nucleation occurs, is also consistent within the obtained error intervals to a pure thermal model, which neglects pressure effects.³⁸

C. Bubble expansion

The initial expansion velocity of the bubble increases with increasing radiant exposure (Fig. 9). Typical velocities ranging from 10 m/s for $180 \text{ mJ}/\text{cm}^2$ up to 85 m/s for $1 \text{ J}/\text{cm}^2$ have been extracted from Figs. 4–6 and are summarized in Table III. This initial bubble expansion velocity increases almost linearly with the applied radiant exposure. For explosive vaporization on rapidly heated surfaces, similar boiling front velocities of a few tens of m/s have been observed experimentally (in different geometries)^{9,50} and have also been modeled by molecular dynamics simulations.⁵⁵

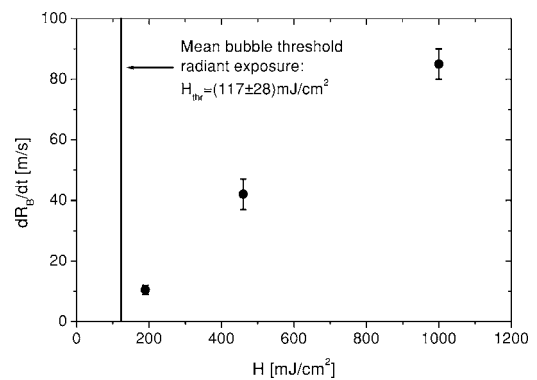


FIG. 9. (Color online) Initial bubble expansion velocities obtained from Figs. 4–6 as a function of the applied radiant exposure.

TABLE III. Bubble expansion velocity extracted from Figs. 4–6 and the corresponding nucleation temperatures $T_{\text{nuc,Rayleigh}}$, which are calculated according to Eq. (4). For comparison, the intervals for the nucleation temperature T_{nuc} deduced from the thermal model (Table II) are listed.

H (mJ/cm ²)	dR/dt (m/s)	$T_{\text{nuc,Rayleigh}}$ (°C)	T_{nuc} (°C)
180	10.5±1.5	128±6	136–254
460	42±4	220±9	112–277
1000	85±5	294±7	120–1030

According to the analytic theory of inertia limited bubble dynamics, the asymptotic bubble expansion velocity in strongly uniformly superheated water can be described by

$$\dot{R}_B(T) = \sqrt{\frac{2[p_{\text{sat}}(T) - p_{\infty}]}{3\rho_l(T)}}, \quad (4)$$

if the surface tension at the bubble interface is neglected and a constant vapor pressure $p_{\text{sat}}(T)$ in the bubble is assumed during expansion.⁵⁶ The condition of constant vapor pressure inside the bubble is fulfilled in the early stages of bubble growth in strongly superheated water, when sufficient vaporization takes place at the bubble interface to compensate the pressure decrease in the bubble due to volume expansion. Using the saturated vapor pressure $p_{\text{sat}}(T)$ according to the IAPWS-95 formulation⁴² and the density of metastable (liquid) water at 1 bar $\rho_l(T)$ according to Skripov *et al.*,⁴³ Eq. (4) leads to typical bubble expansion velocities in the range of several 10 m/s (Fig. 10), which are consistent with our experiments. Although the calculated thermoelastic pressure amplitudes are comparable to the saturated vapor pressure at the nucleation temperature $p_{\text{sat}}(136\text{ °C})=3.2$ bars, the tensile stress (Fig. 8) is thought to influence more likely the bubble nucleation rather than the later stages of bubble growth because of its short duration compared to the duration of bubble expansion.

The initial bubble expansion velocities according to Eq. (4) as plotted in Fig. 10 can be compared to the experimentally determined velocities. According to Eq. (4) each measured expansion velocity provides a temperature of the fluid,

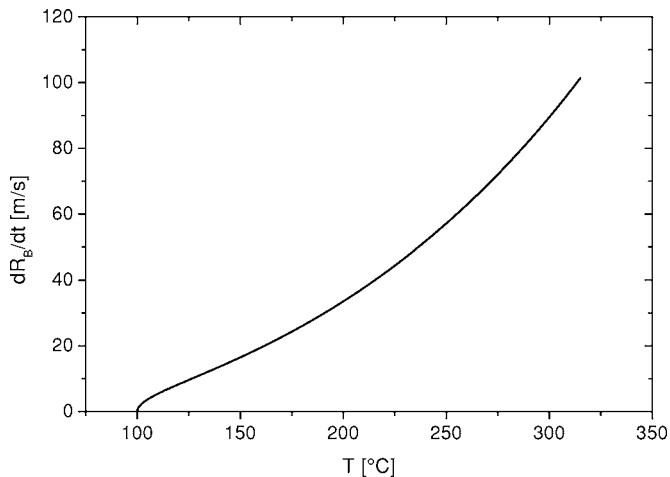


FIG. 10. (Color online) According to Eq. (4) calculated asymptotic bubble expansion velocity for inertia limited dynamics in uniformly superheated water.

in which the bubble expands. The obtained temperatures are listed in Table III and are consistent in most cases with those of Table II, which are deduced from the bubble nucleation experiments. The increase of the bubble expansion velocity with temperature in Table III suggests an increasing nucleation temperature, reaching the spinodal of water at 1 J/cm². The reason for the potentially increasing nucleation temperature might be the compressive stress during the first half of the laser pulse (Fig. 8).

Alternatively, the increasing bubble expansion velocity might be explained by an increasing production of noncondensable gas induced by thermal melanosome disintegration. Irradiation a few times above bubble formation threshold sometimes leads to stable bubbles of noncondensable gas, which is usually explained by thermal disintegration of the melanosome.⁵⁷ Glickman *et al.* have found morphological damage on the surface of bovine RPE melanosomes by scanning electron microscopy (SEM) after multiple irradiations with a 10 ns laser pulse at 214 mJ/cm² ($\lambda=532$ nm).⁵⁸ They hypothesized that vaporization of the melanosome's hydration water, which is released during continuous heating in a temperature range of 100–130 °C,⁵⁹ causes this kind of damage, but it cannot be excluded that vaporization of other melanosome constituents or the bubble collapse causes the morphologic damage. Piattelli and Nicolaus⁴⁷ have observed thermal decarboxylation of melanin, which results in a release of CO₂ during continuous heating of melanin to 140–150 °C. On the other hand, Hayes and Wolbarsht have found no morphologic changes of dog RPE melanosomes by SEM after heating them in standard atmosphere to 350 °C.⁶⁰

IV. CONCLUSION

Nanosecond time-resolved microscopy has been applied to directly image the phase change phenomena and the early stages of the bubble expansion around single micron-sized absorbers heated by 12 ns laser exposure. Porcine retinal pigment epithelial melanosomes, which were heated at rates in the range of 10⁹–10¹¹ K/s, were used for the experiments. The threshold radiant exposure for bubble formation was determined to be 117±28 mJ/cm² at an ambient temperature of 20 °C with a nucleation temperature of $T_{\text{nuc}}=(136\pm23)$ °C. For a radiant exposure of 180 mJ/cm², nucleation was observed at many individual sites on the melanosome's surface. At higher radiant exposures of 460 mJ/cm² and 1 J/cm² a homogeneous bubble formed around the melanosomes during nucleation. The bubble expansion velocity was 10.5 m/s at 180 mJ/cm². It increases almost linearly with a radiant exposure to 85 m/s at 1 J/cm². The magnitude of these velocities suggests that the bubble expansion takes place in strongly superheated water around the melanosome and that the bubble expansion becomes more explosive at increasing radiant exposure, which can lead to a larger damage range in the tissue. The obtained experimental data can be used to verify models for the phase transition of highly superheated water at rapidly heated surfaces, especially with respect to the laser tissue interaction in the retina.

ACKNOWLEDGMENT

One of the authors (J.N.) is partially supported by a fellowship of the FAZIT-Stiftung, Frankfurt am Main, Germany.

- ¹J. Roeder, R. Brinkmann, and R. Birngruber, in *Lasers in Ophthalmology: Basic, Diagnostic and Surgical Aspects*, edited by F. Fankhauser and S. Kwasniewska (Kugler, The Hague, 2003), pp. 119–129.
- ²G. Schüle, H. Elsner, C. Framme, J. Roeder, R. Birngruber, and R. Brinkmann, *J. Biomed. Opt.* **10**, 064022 (2005).
- ³R. Brinkmann *et al.*, *Ophthalmologie* **103**, 839 (2006).
- ⁴M. A. Latina, S. A. B. Sibayan, D. H. Shin, R. J. Noecker, and G. Marcellino, *Ophthalmology* **105**, 2082 (1998).
- ⁵C. M. Pitsillides, E. K. Joe, X. Wei, R. R. Anderson, and C. P. Lin, *Biophys. J.* **84**, 4023 (2003).
- ⁶C. P. Yao, R. Rahmzadeh, E. Endl, Z. Zhang, G. Gerdes, and G. Hüttmann, *J. Biomed. Opt.* **10**, 019506 (2005).
- ⁷V. P. Zharov, K. E. Mercer, E. N. Galitovskaya, and M. E. Smeltzer, *Biophys. J.* **90**, 619 (2006).
- ⁸R. R. Allen, J. D. Meyer, and W. R. Knight, *Hewlett-Packard J.* **36**, 21 (1985).
- ⁹F. Lang, P. Leiderer, and S. Georgiou, *Appl. Phys. Lett.* **85**, 2759 (2004).
- ¹⁰R. C. Hollins, *Curr. Opin. Solid State Mater. Sci.* **4**, 189 (1999).
- ¹¹G. Eyring and M. D. Fayer, *J. Appl. Phys.* **55**, 4072 (1984).
- ¹²J. R. Adleman, H. A. Eggert, K. Buse, and D. Psaltis, *Opt. Lett.* **31**, 447 (2006).
- ¹³C. M. Lawson, G. W. Euliss, and R. R. Michael, *Appl. Phys. Lett.* **58**, 2195 (1991).
- ¹⁴M. Schürenberg, K. Dreisewerd, and F. Hillenkamp, *Anal. Chem.* **71**, 221 (1999).
- ¹⁵Y. Dou, N. Winograd, B. Garrison, and L. V. Zhigilei, *J. Phys. Chem. B* **107**, 2362 (2003).
- ¹⁶T. E. McGrath, G. J. Diebold, D. M. Bartels, and R. A. Crowell, *J. Phys. Chem. A* **106**, 10072 (2002).
- ¹⁷R. R. Anderson and J. A. Parrish, *Science* **220**, 524 (1983).
- ¹⁸G. Hüttmann, B. Radt, J. Serbin, and R. Birngruber, *Proc. SPIE* **5142**, 88 (2003).
- ¹⁹Y. Iida, K. Okuyama, and K. Sakurai, *Int. J. Heat Mass Transfer* **37**, 2771 (1994).
- ²⁰C. T. Avedisian, W. S. Osborne, F. D. McLeod, and C. M. Curley, *Proc. R. Soc. London, Ser. A* **455**, 3875 (1999).
- ²¹C. T. Avedisian, R. E. Cavicchi, and M. J. Tarlov, *Rev. Sci. Instrum.* **77**, 063706 (2006).
- ²²K. J. McEwan, P. K. Milsom, and D. B. James, *Proc. SPIE* **3472**, 42 (1998).
- ²³L. Vivien, D. Riehl, E. Anglaret, and F. Hache, *IEEE J. Quantum Electron.* **36**, 680 (2000).
- ²⁴R. Goedert, R. Becker, A. Clements, and T. Whittaker III, *J. Opt. Soc. Am. B* **15**, 1442 (1998).
- ²⁵L. Vivien, J. Moreau, D. Riehl, P. A. Alloncle, M. Autric, F. Hache, and E. Anglaret, *J. Opt. Soc. Am. B* **19**, 2665 (2002).
- ²⁶C. P. Lin and M. W. Kelly, *Appl. Phys. Lett.* **72**, 1 (1998).
- ²⁷J. Neumann and R. Brinkmann, *Proc. SPIE* **5142**, 82 (2003).
- ²⁸V. P. Zharov, V. Galitovsky, and M. Viegas, *Appl. Phys. Lett.* **83**, 4897 (2003).
- ²⁹D. O. Lapotko and E. Y. Lukianova, *Int. J. Heat Mass Transfer* **48**, 227 (2005).
- ³⁰V. Kotaidis and A. Plech, *Appl. Phys. Lett.* **87**, 213102 (2005).
- ³¹V. Kotaidis, C. Dahmen, G. von Plessen, F. Springer, and A. Plech, *J. Chem. Phys.* **124**, 184702 (2006).
- ³²L. Vivien, D. Riehl, F. Hache, and E. Anglaret, *J. Nonlinear Opt. Phys. Mater.* **9**, 297 (2000).
- ³³V. K. Pustovalov, *Int. J. Heat Mass Transfer* **36**, 391 (1993).
- ³⁴E. Faraggi, B. S. Gerstman, and J. Sun, *J. Biomed. Opt.* **10**, 064029 (2005).
- ³⁵I. M. Belousova, N. G. Mironova, and M. S. Yur'ev, *Opt. Spectrosc.* **94**, 93 (2003).
- ³⁶R. Brinkmann, J. Roeder, and R. Birngruber, *Bull. Soc. Belge Ophtalmol* **302**, 51 (2006).
- ³⁷C. P. Lin, in *Lasers in Ophthalmology: Basic, Diagnostic and Surgical Aspects*, edited by F. Fankhauser and S. Kwasniewska (Kugler, The Hague, 2003), pp. 91–98.
- ³⁸J. Neumann and R. Brinkmann, *J. Biomed. Opt.* **10**, 024001 (2005).
- ³⁹J. Neumann and R. Brinkmann, *J. Biomed. Opt.* **11**, 041112 (2006).
- ⁴⁰J. Neumann and R. Brinkmann, *Proc. SPIE* **5863**, 19 (2005).
- ⁴¹M. L. Wolbarsht, A. W. Walsh, and G. George, *Appl. Opt.* **20**, 2184 (1981).
- ⁴²The IAPWS Formulation 1995 for the Thermodynamic Properties of Ordinary Water Substance for General and Scientific Use, The International Association for Properties of Water and Steam (IAPWS) (1995) (www.iapws.org).
- ⁴³V. P. Skripov, E. N. Sinitsyn, P. A. Pavlov, G. V. Ermakov, G. N. Muratov, N. V. Bulanov, and V. G. Baidakov, *Thermophysical Properties of Liquids in the Metastable (Superheated) State* (Gordon and Breach, New York, 1988).
- ⁴⁴Revised Release on the IAPS Formulation 1985 for the Thermal Conductivity of Ordinary Water Substance, The International Association for Properties of Water and Steam (IAPWS), London, UK, 1998 (www.iapws.org).
- ⁴⁵S. L. Jacques and D. J. McAuliffe, *Photochem. Photobiol.* **53**, 769 (1991).
- ⁴⁶V. P. Zharov, R. R. Letfullin, and E. N. Galitovskaya, *J. Phys. D* **38**, 2571 (2005).
- ⁴⁷M. Piattelli and R. A. Nicolaus, *Tetrahedron* **15**, 66 (1961).
- ⁴⁸V. P. Carey, *Liquid-Vapor Phase Change Phenomena* (Hemisphere, New York, 1992).
- ⁴⁹C. T. Avedisian, *J. Phys. Chem. Ref. Data* **14**, 695 (1985).
- ⁵⁰K. M. Balss, C. T. Avedisian, R. E. Cavicchi, and M. J. Tarlov, *Langmuir* **21**, 10459 (2005).
- ⁵¹*CRC Handbook of Chemistry and Physics*, 76th ed., edited by D. R. Lide (CRC, Boca Raton, FL, 1995).
- ⁵²G. Paltauf and P. E. Dyer, *Chem. Rev. (Washington, D.C.)* **103**, 487 (2003).
- ⁵³A. Vogel and V. Venugopalan, *Chem. Rev. (Washington, D.C.)* **103**, 577 (2003).
- ⁵⁴M. I. Kahn and G. J. Diebold, *Ultrasonics* **33**, 265 (1995).
- ⁵⁵Y. Dou, L. V. Zhigilei, N. Winograd, and B. Garrison, *J. Phys. Chem. A* **105**, 2748 (2001).
- ⁵⁶M. S. Plesset and A. Prosperetti, *Annu. Rev. Fluid Mech.* **9**, 145 (1977).
- ⁵⁷J. Neumann and R. Brinkmann, *Proc. SPIE* **4617**, 180 (2002).
- ⁵⁸R. D. Glickman, S. L. Jacques, R. T. Hall, and N. Kumar, *Proc. SPIE* **4257**, 134 (2001).
- ⁵⁹P. Baraldi, R. Capelletti, P. R. Crippa, and N. Romeo, *J. Electrochem. Soc.* **126**, 1207 (1979).
- ⁶⁰J. R. Hayes and M. L. Wolbarsht, *Aerosp. Med.* **39**, 474 (1968).
- ⁶¹I. A. Vitkin, J. Woolsley, B. C. Wilson, and R. R. Anderson, *Photochem. Photobiol.* **59**, 455 (1994).